Article

Binding of Genistein to the Estrogen Receptor Based on an Experimental Electron Density Study

Eric J. Yearley, Elizabeth A. Zhurova, Vladimir V. Zhurov, and A. Alan Pinkerton

J. Am. Chem. Soc., **2007**, 129 (48), 15013-15021 • DOI: 10.1021/ja075211j

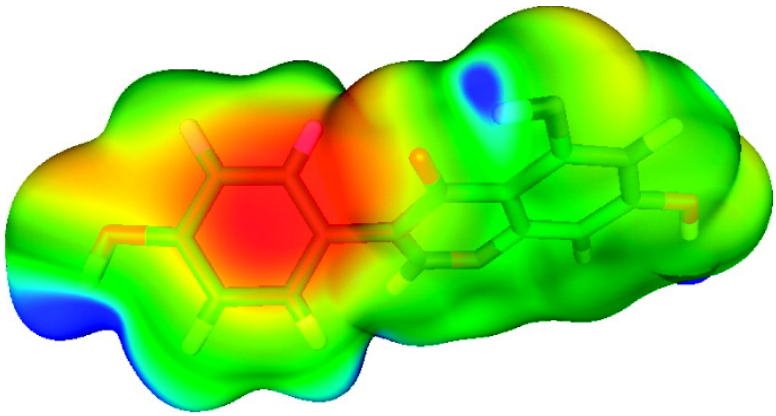

J|A|C|S
ARTICLES
Published on Web 11/10/2007

Binding of Genistein to the Estrogen Receptor Based on an Experimental Electron Density Study

Eric J. Yearley, Elizabeth A. Zhurova, Vladimir V. Zhurov, and A. Alan Pinkerton*

Contribution from the Department of Chemistry, University of Toledo, Toledo, Ohio 43606

Received July 12, 2007; E-mail: apinker@uoft02.utoledo.edu

Abstract: In a continuing effort to determine a relationship between the biological function and the electronic properties of steroidal and nonsteroidal estrogens by analysis of the submolecular properties, an experimental charge density study has been pursued on the nonsteroidal phytoestrogen, genistein. X-ray diffraction data were obtained using a Rigaku R-Axis Rapid high-power rotating anode diffractometer with a curved image plate detector at 20(1) K. The total electron density was modeled using the Hansen−Coppens multipole model. Genistein packs in puckered sheets characterized by intra- and intermolecular hydrogen bonds while weaker intermolecular hydrogen bonds (O···H−C) exist between the sheets. A topological analysis of the electron density of genistein was then completed to characterize all covalent bonds, three O···H−O and four O···H−C intermolecular hydrogen bonds. Two O···H−O hydrogen bonds are incipient (partially covalent) type bonds, while the other O···H−O hydrogen bond and O···H−C hydrogen bonds are of the pure closed-shell interaction type. In addition, two intermolecular H···H interactions have also been characterized from the topology of the electron density. The binding of genistein to the estrogen receptor is discussed in terms of the electrostatic potential derived from the electron density distribution.

1. Introduction

Phytoestrogens are plant products with estrogen-like activity. Recently, a significant amount of research has been initiated on these compounds because of their potential health benefits ranging from treatment of cardiovascular diseases to hormone-dependent breast cancer.[1]

One phytoestrogen that has generated interest is genistein (Figure 1). The interest in this molecule, like other phytoestrogens, stems from the potential health benefits that it might provide.[3] Based on recent reports, genistein may have positive health benefits in estrogen-related problems such as menopause and osteoporosis,[4−6] amyloid diseases,[7] cardiovascular diseases,[8,9] and even breast cancer[10,11] where genistein has been found to inhibit certain pathways necessary for tumor growth. The potential positive benefits of genistein for breast cancer

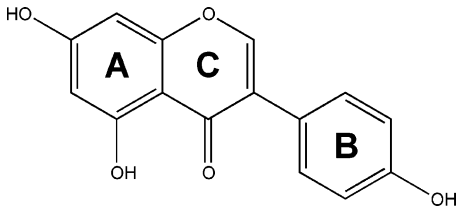

Figure 1. Representation of the genistein molecule.[2]

treatment were first surmised by Lee et al.[10] when they found lower incidences of breast cancer in Asian women in comparison to American women. Since Asian women traditionally have a diet rich in soy products, and genistein is present in many of these products, it was suggested that genistein might manifest some anticancer properties.

Furthermore, there has been additional discussion about the antiestrogenic properties of genistein in the last several years. Does genistein hinder or promote breast cancer cell growth? Several studies seemed to point to both conclusions. The experimental evidence, from a number of recent studies, suggests that genistein has a biphasic effect on the growth of the breast cancer cell depending on the concentration or dose of genistein.[11]

We have recently initiated studies to develop correlations between the electronic properties of compounds that hinder or promote breast cancer growth and their biological functions.[12,13] It has been previously suggested[14,15] that the variance of activity

(1) Cos, P.; De Bruyne, T.; Apers, S.; Berghe, D. V.; Pieters, L.; Vlietinck, A. J. *Planta Med.* **2003**, *69*, 589.
(2) Stafford, H. A. *Flavonoid Metabolism*; CRC Press: Boca Raton, Fl, 1990.
(3) Dixon, R. A.; Ferreira, D. *Phytochemistry* **2002**, *60*, 205.
(4) Beck, V.; Rohr, U.; Jungbauer, A. *J. Steroid Biochem. Mol. Biol.* **2005**, *94*, 499.
(5) Morabito, N.; Crisafulli, A.; Vergara, C.; Gaudio, A.; Lasco, A.; Frisina, N.; D'Anna, R.; Corrado, F.; Pizzoleo, M. A.; Cincotta, M.; Altavilla, D.; Ientile, R.; Squadrito, F. *J. Bone Miner. Res.* **2002**, *17*, 1904.
(6) Crisafulli, A.; Altavilla, D.; Squadrito, G.; Romeo, A.; Adamo, E. B.; Marini, R.; Inferrera, M. A.; Marini, H.; Bitto, A.; D'Anna, R.; Corrado, F.; Bartolone, S.; Frisina, N.; Squadrito, F. *J Clin. Endocrinol. Metab.* **2004**, *89*, 188.
(7) Green, N. S.; Foss, T. R.; Kelly, J. W. *PNAS* **2005**, *102*, 14545.
(8) Hwang, J.-T.; Park, I.-J.; Shin, J.-I.; Lee, Y. K.; Lee, S. K.; Baik, H. W.; Ha, J.; Park, O. J. *Biochem. Biophys. Res. Commun.* **2005**, *338*, 694.
(9) Szkudelska, K.; Nogowski, L.; Szkudelski, T. *J. Steroid Biochem. Mol. Biol.* **2000**, *75*, 265.
(10) Lee, H. P.; Gourley, L.; Duffy, S. W.; Esteve, J.; Lee, J.; Day, N. E. *Lancet* **1991**, *337*, 1197.
(11) Matsumura, A.; Ghosh, A.; Pope, G. S.; Darbre, P. D. *J. Steroid Biochem. Mol. Biol.* **2005**, *94*, 431.
(12) Zhurova, E. A.; Matta, C. F.; Wu, N.; Zhurov, V. V.; Pinkerton, A. A. *J. Am. Chem. Soc.* **2006**, *128*, 8849.
(13) Parrish, D. A.; Zhurova, E. A.; Kirschbaum, K.; Pinkerton, A. A. *J. Phys. Chem. B* **2006**, *110*, 26442.
(14) VanderKuur, J. A.; Hafner, M. S.; Christman, J. K.; Brooks, S. C. *Biochemistry* **1993**, *32*, 7016.
(15) VanderKuur, J. A.; Wiese, T.; Brooks, S. C. *Biochemistry* **1993**, *32*, 7002.

(promoting or hindering breast cancer growth) between these compounds is the result of alterations in the molecular electrostatic potential generated by small differences in the molecular structure. The differences generated by different interactions of the phenolic oxygen and the π electrons of the aromatic rings in steroidal and nonsteroidal estrogens may determine whether a compound will hinder or promote breast cancer. Recently, Brooks and Skafar[16] have suggested, through a number of molecular models of agonistic and antagonistic ligands complexed with the estrogen receptor, that small changes in the molecular conformations of the ligand may lead to altered conformations in the estrogen receptor and therefore lead to a modification in gene transcription and biological activity. It was also observed that the H12 region of the estrogen receptor complexed with 4-hydroxy-estratriene-17β-ol was not able to clamp down over the ligand binding cavity.[16] This may prevent co-activators from binding to this complex and, thus, engender a decrease in gene transcription. Accordingly, a number of studies focused on steroidal and nonsteroidal estrogenic molecules have been initiated in our group to experimentally examine the hypothesis that the details of the electrostatic potential may determine whether a compound will hinder or promote breast cancer.[12,13]

Genistein has been chosen for charge density analysis for several chemical and crystallographic reasons. Because of its recent interest to the medical field, especially in the area of breast cancer research, a charge density analysis will provide significant insight into the properties of the molecule as the total electron density distribution defines all the molecular properties in the ground state,[17] including the electrostatic potential. This analysis should lead to a better understanding of how the genistein molecule approaches and binds to the estrogen receptor thus adding another element to the larger study of breast cancer related compounds using charge density measurements.[12,13] Genistein is also commercially available, and the crystallization methods have been documented.[18] In addition, the genistein molecule is a small, nonsteroidal estrogen-like compound that crystallizes in a centrosymmetric space group allowing us to obtain a more reliable model for the electron density distribution and, hence, the electrostatic potential than for most naturally occurring estrogens.

2. Experimental Details

Colorless crystals of genistein were prepared as previously described.[18] A crystal (0.26 × 0.24 × 0.11 mm^3) was glued to a 0.10 mm glass capillary with epoxy resin, mounted on a Rigaku R-Axis Rapid rotating anode (Mo Kα) diffractometer, and cooled to 20(1) K.[19−21]

Intensity data were collected in three different runs for 0°−180° in ω in 4° steps, at $\chi = 26.4°$, $\varphi = -16.2°$; $\chi = 16.4°$, $\varphi = -16.2°$; and $\chi = 0.0°$, $\varphi = 90.0°$.[22] Three similar runs offset by 2° in ω were taken in order to provide an accurate image to image scaling. The exposure time of each frame was 300 s, and the entire measurement was completed in less than 2 days.

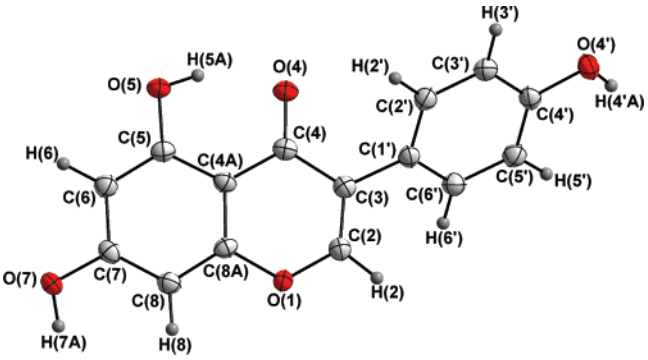

Figure 2. ORTEP drawing of genistein at 20 K showing thermal probability ellipsoids at the 90% probability level for the non-hydrogen atoms

The reflections were indexed using HKL2000,[23] then integrated with the VIIPP program,[24,25] which uses oval integration boxes extended along the radial directions according to the $\alpha_1-\alpha_2$ splitting. Reflections with intensities below $3\sigma(I)$ were deemed unobservable and rejected. The program SORTAV[26] was used to sort and average reflections and to determine outliers. Less than 1.5% of the total number of reflections were considered extreme outliers and removed. The absorption was considered negligible ($\mu = 0.12$ mm^{-1}), and the data were scaled (max. 2.5%) and averaged in the *mmm* point group. Data reduction statistics and crystallographic parameters are summarized.[27]

3. Refinements

The genistein crystal structure has been redetermined with the program SHELXTL,[28] and the results are in good agreement with the previous report.[18] All hydrogens were found from a Fourier difference map. An ORTEP drawing of the genistein molecule is shown in Figure 2.

The electron density analysis was based on the Hansen−Coppens multipole model[29] using XD.[30] First, the coordinates and atomic displacement parameters for the non-hydrogen atoms were refined with high angle data (sin $\theta/\lambda > 0.7$ Å^{-1}), whereas those for the hydrogens were refined using low angle data (sin $\theta/\lambda < 0.7$ Å^{-1}). The C−H and O−H distances were then extended to the appropriate average bond lengths ($C_{sp2}H = 1.083$ Å, OH = 0.967 Å) as obtained from neutron diffraction data.[31] A local atomic coordinate system similar to the one used for

(16) Brooks, S. C.; Skafar, D. F. *Steroids* **2004**, *69*, 401.
(17) Hohenberg, P.; Kohn, W. *Phys. Rev.* **1964**, *136*, B864.
(18) Breton, M.; Precigoux, G.; Courseille, C.; Hospital, M. *Acta Crystallogr.* **1975**, *B31*, 921.
(19) Hardie, M. J.; Kirschbaum, K.; Martin, A.; Pinkerton, A. A. *J. Appl. Crystallogr.* **1998**, *31*, 815.
(20) Ribaud, L.; Wu, G.; Zhang, Y.; Coppens, P. *J. Appl. Crystallogr.* **2001**, *34*, 76.
(21) Kirschbaum, K.; Martin, A.; Parrish, D. A.; Pinkerton, A. A. *J. Phys.: Condens. Matter* **1999**, *11*, 4483.
(22) The first two runs were chosen to be ~5° away from the *c* axis to minimize reflection overlap and multiple scattering. The third run was at a random setting to complete the data set, but many reflections were rejected due to unresolved overlap.
(23) Otwinowski, Z.; Minor, W. *Methods Enzymol. Macromol. Cryst. Part A* **1997**, *276*, 307.
(24) Zhurov, V. V.; Zhurova, E. A.; Chen, Y.-S.; Pinkerton, A. A. *J. Appl. Crystallogr.* **2005**, *38*, 827.
(25) Zhurova, E. A.; Zhurov, V. V.; Tanaka, K. *Acta Crystallogr.* **1999**, *B55*, 917.
(26) Blessing, R. H. *Cryst. Rev.* **1987**, *1*, 3.
(27) Space group, *Pbca*, $a = 6.8384(1)$ Å, $b = 14.4900(2)$ Å, $c = 23.5088(4)$ Å, $Z = 8$, $T = 20(1)$ K, $\lambda = 0.710\,73$ Å, $(\sin\theta/\lambda)_{max} = 1.33$ Å^{-1}, total integrated reflections = 198 896, unique reflections = 15 481, unique reflections included in refinements ($I > 3\sigma(I)$ measured more than twice) = 5373, average redundancy = 12.7, R_{int} ($I > 3\sigma(I)$) = 0.0189, number of parameters = 826, $R(F^2)$(spherical) = 0.0555, $wR_2(F^2)$(spherical) = 0.0949, $R(F)$(multipole) = 0.0146, $R(F^2)$(multipole) = 0.0175, $wR_2(F^2)$(multipole) = 0.0323, GOF = 1.02, residual electron density = −0.090/0.095 e Å^{-3}.
(28) Sheldrick, G. M. *SHELXTL*, v. 6.14; University of Göttingen: Germany, 2000.
(29) Hansen, N. K.; Coppens, P. *Acta Crystallogr.* **1978**, *A34*, 909.
(30) Koritsanszky, T.; Howard, S. T.; Richter, T.; Macchi, P.; Volkov, A.; Gatti, C.; Mallinson, P. R.; Farrugia, L. J.; Su, Z.; Hansen, N. K. *XD: A Computer Program Package for Multipole Refinement and Analysis of Electron Densities from Diffraction Data*; University of Berlin: Germany, 2003.
(31) Allen, F. H.; Kennard, O.; Watson, D. G.; Brammer, L.; Orpen, A. G.; Taylor, R. *J. Chem. Soc., Perkin Trans. 2* **1987**, S1.

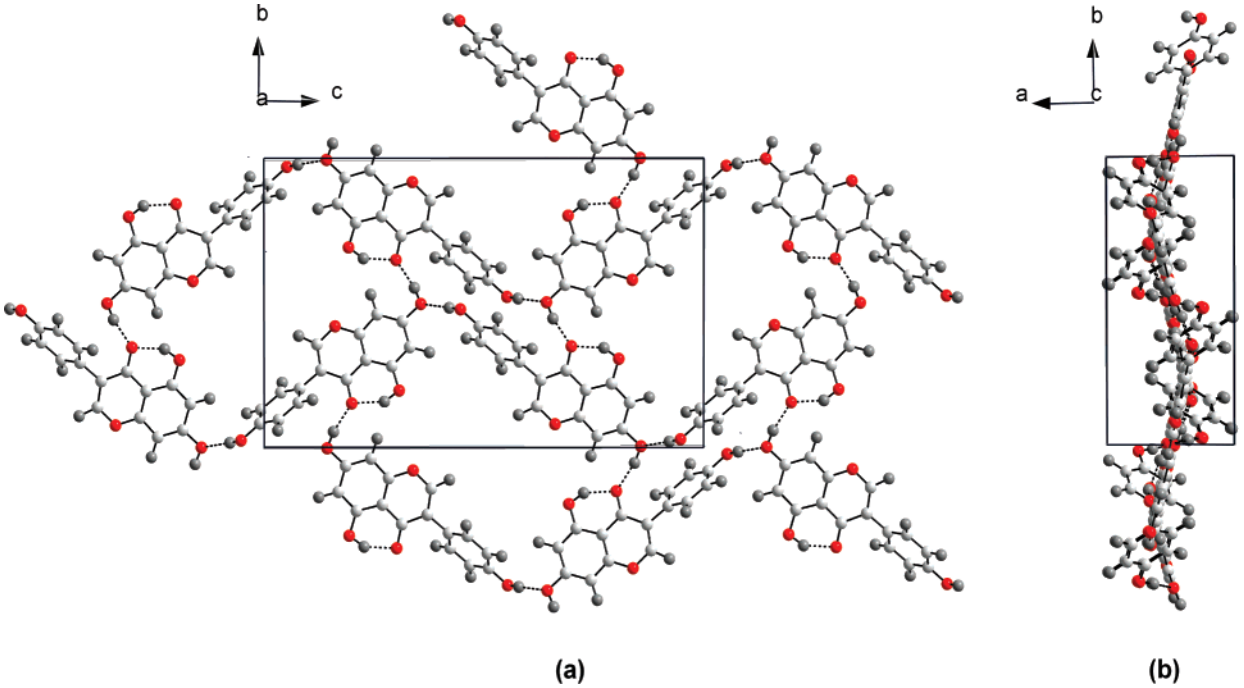

Figure 3. Crystal packing diagram of genistein viewed (a) down the *a*-axis of the unit cell and (b) down the *c*-axis of the unit cell, showing the hydrogen-bonded puckered layers. Oxygen atoms are red, carbon atoms are light gray, and hydrogens are dark gray.

charge density studies of steroidal estrogens was used.[32] Initially, the number of refined parameters was reduced by using chemical constraints and refining only the "most important" multipoles.[32] For the full multipole refinement, oxygen and carbon atoms were treated up to the hexadecapole level, and the hydrogens, to the quadrupole level ($\sin\theta/\lambda < 1.0$ Å^{-1}). The scale factor was refined over all data. All constraints were released progressively, and the final model was unconstrained.

Different contraction and expansion parameters (κ and κ')[29] were assigned to groups of atoms based on their atom type, hybridization, and chemical environment. A total of nine kappa's were implemented into the refinement. The κ and κ' parameters for the hydrogen atoms were fixed to 1.20 during the refinement, and all others were allowed to refine.[33]

A number of different tests have been used to confirm the quality of the diffraction data and of the model.[27] First, the final $R(F^2)$ value converged at 0.0175 for all data. Second, the residual density maps exhibit only small (<0.1 e Å^{-3}), random features.[34] The differences of mean-square displacement amplitudes along the interatomic vectors were[35] $\leq 8 \times 10^{-4}$ (Å^2). Finally, $\Sigma F_{obs}/\Sigma F_{calc}$ vs resolution plotted in 0.05 Å^{-1} intervals was very close to unity (~1.0% deviation for $\sin\theta\lambda \leq 1.0$ Å^{-1}, up to ~2.5% deviation for the highest angle data).

4. Results and Discussion

4.1. Structural Analysis and Packing of Genistein in the Crystalline State. The atomic coordinates and atomic displacement factors of the crystalline structure of genistein have been deposited. The current structure is in very good agreement with the previously reported study,[18] with the A and C rings and their substituents coplanar and the aromatic B ring twisted by 53.8° with respect to A and C. We note that the distance between the two hydroxyl oxygens on opposite sides of genistein in the crystalline state, O(7) and O(4′), is 11.9823(8)Å. As shown before,[12,36,37] the intramolecular distance between the two hydroxyl oxygens of estrogens that readily interact with the estrogen receptor range from ~10 to 12 Å, therefore, the genistein molecule should enter the estrogen receptor and bind in the ligand binding cavity without hindrance.

Genistein packs in puckered sheets perpendicular to *a* (Figure 3) characterized by intra- and intermolecular hydrogen bonds. Weaker intermolecular hydrogen bonds exist between the sheets. All hydrogen bonds have been fully characterized by the topological analysis of the total electron density[38] as described below.

4.2. Deformation Electron Density Maps. The dynamic model deformation electron density (Figure 4) shows peaks associated with the covalent bonds of the genistein molecule and the lone pairs of the oxygens. The average maximum value of the deformation density increases as expected from weaker bonds to stronger bonds. The average values for the maximum value of deformation density for the C−C double bond, the C−C aromatic bonds, and the C−C single bonds are 0.63, 0.54, and 0.52 e Å^{-3}, respectively. The average values for the C−O−C bonds, C−O hydroxyl bonds, and the C−O carbonyl bond are 0.29, 0.31, and 0.42 e Å^{-3}, respectively. The average values for the C−H bonds and the O−H bonds are 0.48 and 0.31 e Å^{-3}.

(32) Kirschbaum, K.; Poomani, K.; Parrish, D. A.; Zhurova, E. A.; Pinkerton, A. A. *J. Appl. Crystallogr.* **2003**, *36*, 1464.
(33) κ and κ': O(1) - 0.995(3), 1.31(7); O(4) - 0.981(3), 0.91(6); O(5), O(7), O(4′) - 0.986(2), 1.00(4); C(5), C(7), C(4′) - 1.009(5), 1.01(2); C(4) - 0.994-(8), 0.91(3); C(2), C(6), C(8), C(2′), C(3′), C(5′), C(6′) - 0.997(3), 1.00-(2); C(3), C(4A), C(8A), C(1′) - 1.008(3), 1.00(2);
(34) Maps have been deposited.
(35) Hirshfeld, F. L. *Acta Crystallogr.* **1976**, *A32*, 239.
(36) Fukuzawa, K.; Kitaura, K. Uebayasi, M.; Nakata, K.; Kaminuma, T.; Nakano, T. *J. Comput. Chem.* **2005**, *26*, 1.
(37) Brueggemeier, R. W.; Miller, D. D.; Dalton, J. T. In *Foye's Principles of Medicinal Chemistry*, 5th ed.; Williams, D. A., Lemke, T. L., Eds.; Lippincott Williams and Wilkins: Philadelphia, 2002.
(38) Bader, R. F. W. In *Atoms in Molecules: A Quantum Theory*; Halpen, J., Green, M. L. H., Eds.; *The International Series of Monographs of Chemistry*; Clarendon Press: Oxford, 1990.

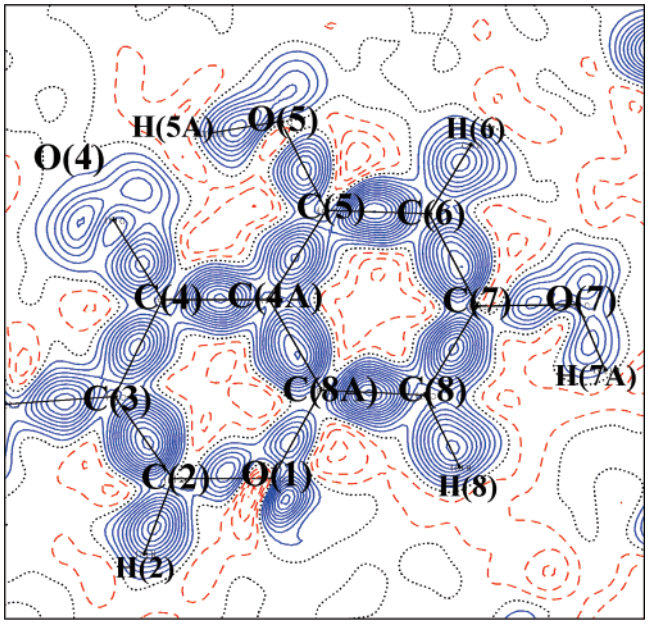

(a)

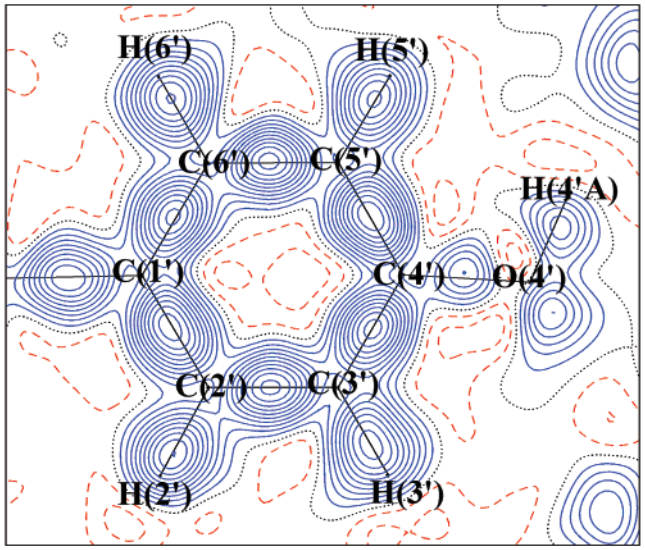

(b)

Figure 4. Dynamic model deformation density map of the (a) A and C rings and (b) the B ring with contour intervals 0.05 e Å^{-3}: solid blue lines, positive; dashed red lines, negative; and dotted black lines, zero. Fourier series are truncated at 1.0 Å^{-1}.

4.3. Topological Analysis of the Total Electron Density. A topological analysis[38] of the total electron density was performed using the WinXPRO[39,40] program. The (3,−1) bonding intramolecular critical points (CP) are listed in Table 1. For the heteronuclear bonds, the CPs in the electron density (ρ_{cp}) are in closer proximity to the least electronegative atom indicating polarization of the bonds as expected. For the homonuclear bonds (C−C), the bond critical point is very close to the center of the bond.

The Laplacian values at all these CPs are negative indicating a shared interaction (covalent) type. The ρ_{cp} value increases as expected from C−C single bonds to C−C double bonds. The average ρ_{cp} values for the C−C double bond, the C−C aromatic bonds, and the C−C single bonds are 2.36, 2.12, and 1.90 e Å^{-3}, respectively. The average ρ_{cp} values for the C−O−C bonds, C−O hydroxyl bonds, and the C−O carbonyl bond are 2.07, 2.15, and 2.62 e Å^{-3}, respectively. The average ρ_{cp} values for the C−H aromatic bonds and the O−H hydroxyl bonds are 1.91 and 2.28 e Å^{-3}, respectively. Finally, the ellipticity (ϵ) of the bond increases with increasing π character from close to zero in the C−C single bonds to ∼0.2 for the C−C multiple bonds. The topological property values at the CPs are comparable to those for similar types of bonds found for other molecules reported in recently completed charge density studies.[12,13,41−50]

The properties of the (3,−1) bond CPs for all hydrogen bonds are listed in Table 2. For every hydrogen bond, the presence of a (3,−1) CP and the corresponding virial path[51,52] has been confirmed. In the original paper on the crystal structure of genistein, three strong O···H−O hydrogen bonds were reported. These three O···H−O bonds are confirmed by the current topological analysis, but in addition, four weaker O···H−C hydrogen bonds have also been found and characterized.

Of the three strong O···H−O hydrogen bonds, the carbonyl oxygen, O(4), is an acceptor for two O···H−O bonds, one of which is an intramolecular hydrogen bond between O(4) and H(5A)−O(5) and the other an intermolecular hydrogen bond between O(4) and H(7A)^{i}−O(7)^{i}.[53] As for the last O···H−O bond, the hydroxyl oxygen, O(7), acts as an acceptor when participating in a hydrogen bond with the H(4′A)^{ii}−O(4′)^{ii} donor group (Figure 5). Each of these O···H−O hydrogen bonds are relatively short ranging from 1.748 to 1.865 Å.

O···H−C type hydrogen bonds were found between O(5) and H(2′)^{iii}−C(2′)^{iii} and between O(4) and H(8)^{i}−C(8)^{i}. In addition, O(4′) serves as an acceptor for two O···H−C hydrogen bonds between H(2)^{iv}−C(2)^{iv} and H(3′)^{v}−C(3′)^{v}. Each of these O···H−C hydrogen bonds were at distances ranging from 2.303 to 2.622 Å. For all hydrogen bonds, the low electron density (compared to the covalent bonds) and a positive Laplacian at the bond CPs are reported in Table 2.

The analysis of the local kinetic (g), potential (v), and electronic (h_e) energies[54−56] at bond CPs allows for further

(39) Stash, A. I.; Tsirelson, V. G. *Crystallogr. Rep.* **2005**, *50*, 177.
(40) Stash, A. I.; Tsirelson, V. G. *J. Appl. Crystallogr.* **2002**, *35*, 371.
(41) Messerschmidt, M.; Scheins, S.; Luger, P. *Acta Crystallogr.* **2005**, *B61*, 115.
(42) Chęcińska, L.; Mebs, S.; Hübschle, C. B.; Förster, D.; Morgenroth, W.; Luger, P. *Org. Biomol. Chem.* **2006**, *4*, 3242.
(43) Oddershede, J.; Larsen, S. *J. Phys. Chem. A* **2004**, *108*, 1057.
(44) Destro, R.; Soave, R.; Barzaghi, M.; Presti, L. L. *Chem.—Eur. J.* **2005**, *11*, 4621.
(45) Guillot, R.; Muzet, N.; Dahaoui, S.; Lecomte, C.; Jelsch, C. *Acta Crystallogr.* **2001**, *B57*, 567.
(46) Benabicha, F.; Pichon-Pesme, V.; Jelsch, C.; Lecomte, C.; Khmou, A. *Acta Crystallogr.* **2000**, *B56*, 155.
(47) Coppens, P.; Abramov, Y.; Carducci, M.; Korjov, B.; Novozhilova, I.; Alhambra, C.; Pressprich, M. R. *J. Am. Chem. Soc.* **1999**, *121*, 2585.
(48) Arnold, W. D.; Sanders, L. K.; McMahon, M. T.; Volkov, A. V.; Wu, G.; Coppens, P.; Wilson, S. R.; Godbout, N.; Oldfield, E. *J. Am. Chem. Soc.* **2000**, *122*, 4708.
(49) Wagner, A.; Flaig, R.; Dittrich, B.; Schmidt, H.; Koritsánszky, T.; Luger, P. *Chem.—Eur. J.* **2004**, *10*, 2977.
(50) Rödel, E.; Messerschmidt, M.; Dittrich, B.; Luger, P. *Org. Biomol. Chem.* **2006**, *4*, 475.
(51) Bader, R. F. W. *J. Phys. Chem.* **1998**, *A102*, 7314.
(52) Zhurova, E. A.; Tsirelson, V. G.; Stash, A. I.; Yakovlev, M. V.; Pinkerton, A. A. *J. Phys. Chem. B* **2004**, *108*, 20173.
(53) Symmetry operations: (i) $1-x, y-{}^1/_2, -z+{}^1/_2$; (ii) $x, -y+{}^1/_2, z+{}^1/_2$; (iii) $x+{}^1/_2, y, -z+{}^1/_2$; (iv) $x-{}^1/_2, -y+{}^1/_2, -z$; (v) $-x, -y, -z$.
(54) Tsirelson, V. G. *Acta Crystallogr.* **2002**, *B58*, 632.
(55) Abramov, Y. A. *Acta Crystallogr.* **1997**, *A53*, 264.
(56) Kirzhnits, D. A. *Sov. Phys. JETP.* **1957**, *5*, 64.

Table 1. Critical Point Properties of the Covalent Bonds in Genistein[a]

bond path	ρ (e Å^{-3})	$\nabla^2\rho$ (e Å^{-5})	λ_1 (e Å^{-5})	λ_2 (e Å^{-5})	λ_3 (e Å^{-5})	R_{ij} (Å)	d_1 (Å)	d_2 (Å)	ϵ
O(4)−C(4)	2.622	−29.07	−22.578	−21.892	15.398	1.262	0.809	0.453	0.031
O(7)−C(7)	2.097	−21.82	−18.457	−16.223	12.862	1.356	0.830	0.527	0.138
O(5)−C(5)	2.262	−24.20	−20.464	−18.630	14.893	1.347	0.805	0.542	0.098
O(4′)−C(4′)	2.092	−19.60	−17.622	−16.432	14.458	1.363	0.813	0.550	0.072
O(1)−C(8A)	1.982	−20.13	−17.214	−15.191	12.274	1.365	0.852	0.513	0.133
O(1)−C(2)	2.162	−24.77	−18.540	−17.966	11.739	1.345	0.826	0.519	0.032
C(7)−C(6)	2.141	−19.16	−16.958	−14.074	11.876	1.406	0.744	0.663	0.205
C(6)−C(5)	2.193	−20.74	−18.069	−14.116	11.444	1.386	0.669	0.717	0.280
C(5)−C(4A)	1.977	−15.72	−15.005	−12.976	12.258	1.426	0.695	0.730	0.156
C(4A)−C(8A)	2.139	−18.08	−16.414	−14.224	12.554	1.404	0.686	0.718	0.154
C(8A)−C(8)	2.191	−21.02	−17.763	−14.479	11.221	1.388	0.730	0.659	0.227
C(8)−C(7)	2.138	−18.78	−16.647	−14.033	11.898	1.395	0.688	0.708	0.186
C(1′)−C(2′)	2.133	−18.52	−16.709	−13.898	12.083	1.403	0.718	0.686	0.202
C(2′)−C(3′)	2.120	−18.40	−16.215	−13.707	11.526	1.389	0.696	0.693	0.183
C(3′)−C(4′)	2.065	−16.40	−15.835	−12.536	11.970	1.401	0.669	0.733	0.263
C(4′)−C(5′)	2.192	−20.40	−17.732	−14.578	11.907	1.397	0.699	0.698	0.216
C(5′)−C(6′)	2.083	−17.54	−15.980	−13.058	11.495	1.398	0.682	0.717	0.224
C(6′)−C(1′)	2.048	−14.79	−14.927	−12.325	12.459	1.401	0.710	0.691	0.211
C(3)−C(1′)	1.789	−12.76	−12.752	−12.296	12.284	1.480	0.752	0.727	0.037
C(4)−C(3)	1.905	−15.47	−14.148	−12.485	11.167	1.455	0.733	0.722	0.133
C(4A)−C(4)	2.009	−18.41	−15.764	−13.456	10.814	1.443	0.738	0.704	0.171
C(3)−C(2)	2.357	−23.14	−19.027	−15.563	11.449	1.357	0.652	0.705	0.223
(H7A)−O(7)	2.266	−40.26	−39.056	−37.621	36.416	0.967	0.208	0.760	0.038
(H5A)−O(5)	2.349	−40.67	−40.136	−38.518	37.983	0.967	0.209	0.760	0.042
H(4′A)−O(4′)	2.239	−33.43	−35.619	−34.748	36.937	0.967	0.220	0.747	0.025
H(6)−C(6)	1.822	−15.62	−16.278	−15.682	16.341	1.083	0.405	0.678	0.038
H(2)−C(2)	1.993	−23.47	−20.558	−19.457	16.547	1.083	0.368	0.717	0.057
H(8)−C(8)	1.911	−19.89	−18.142	−17.168	15.417	1.083	0.398	0.686	0.057
H(2′)−C(2′)	1.880	−18.39	−17.437	−16.276	15.328	1.083	0.408	0.675	0.071
H(3′)−C(3′)	1.880	−18.40	−19.050	−17.852	18.503	1.083	0.351	0.733	0.067
H(5′)−C(5′)	1.854	−17.05	−17.063	−15.622	15.632	1.083	0.412	0.671	0.092
H(6′)−C(6′)	1.998	−22.87	−19.368	−17.510	14.012	1.083	0.425	0.659	0.106

[a] ρ is the electron density; $\nabla^2\rho$ is the Laplacian where $\nabla^2\rho = \lambda_1 + \lambda_2 + \lambda_3$; λ_1, λ_2, and λ_3 are the principal curvatures; d_1 and d_2 are the distances from the bond critical point to atoms 1 and 2, respectively; R is the interatomic distance; ϵ is the ellipticity, where $\epsilon = (\lambda_1/\lambda_2) - 1$.

Table 2. Critical Point Properties of the Hydrogen Bonds and H···H Interactions[a]

bond path	ρ (e Å^{-3})	$\nabla^2\rho$ (e Å^{-5})	λ_1 (e Å^{-5})	λ_2 (e Å^{-5})	λ_3 (e Å^{-5})	R_{ij} (Å)	d_1 (Å)	d_2 (Å)	g (au)	v (au)	h_e (au)	D (kcal/mol)
O(4)···H(5A)−O(5)	0.288	3.72	−1.840	−1.517	7.073	1.748	1.132	0.621	0.0406	−0.0427	−0.0021	13.40
O(4)···H(7A)−O(7)^{i}	0.242	2.41	−1.623	−1.473	5.509	1.801	1.167	0.635	0.0279	−0.0308	−0.0029	9.66
O(7)···H(4′A)−O(4′)^{ii}	0.181	2.52	−1.132	−0.997	4.652	1.865	1.210	0.658	0.0243	−0.0225	0.0018	7.06
O(4)···H(8)−C(8)^{i}	0.049	1.34	−0.139	−0.073	1.552	2.387	1.441	0.960	0.0101	−0.0062	0.0039	1.95
O(4′)···H(3′)−C(3′)^{v}	0.058	1.17	−0.214	−0.194	1.583	2.303	1.414	0.908	0.0091	−0.0061	0.0030	1.91
O(4′)···H(2)−C(2)^{iv}	0.054	0.96	−0.192	−0.142	1.293	2.437	1.465	0.979	0.0076	−0.0052	0.0024	1.63
O(5)···H(2′)−C(2′)^{iii}	0.026	0.45	−0.109	−0.084	0.638	2.622	1.589	1.055	0.0034	−0.0021	0.0013	0.66
H(3′)···H(3′)^{v}	0.051	0.67	−0.161	−0.132	0.963	2.179	1.089	1.089	0.0055	−0.0040	0.0015	-
H(6)···H(5′)^{ii}	0.033	0.56	−0.112	−0.089	0.761	2.402	1.092	1.325	0.0043	−0.0027	0.0015	-

[a] Symmetry operators: see ref 53. ρ is the electron density; $\nabla^2\rho$ is the Laplacian where $\nabla^2\rho = \lambda_1 + \lambda_2 + \lambda_3$; λ_1, λ_2, and λ_3 are the principal curvatures; d_1 and d_2 are the distances from the bond critical point to atoms 1 and 2, respectively; R is the O···H or H···H distance; g, v, h_e are the kinetic, potential, and total electronic energy densities;[54−56] $D = -v/2$ is the dissociation energy.[57]

classification of the hydrogen bonds in the genistein crystal. The first two O···H−O bonds involving the carbonyl oxygen (Table 2) have relatively small electron density values (0.29 and 0.24 e Å^{-3}), $\nabla^2\rho > 0$, $1 < |v|/g < 2$ and $h_e < 0$, which point to an incipient (partially covalent) type of bonding. The rest of the hydrogen bonds have $\nabla^2\rho > 0$, but $|v|/g < 1$ and $h_e > 0$, which are indicators of a pure closed-shell interaction type.[58] These bonds, in particular those of the O···H−C type, are weaker as seen from the dissociation energy values[57] reported in Table 2.

We also note that two local concentrations of electrons associated with lone pairs have been found around every oxygen atom, except for O(7) which exhibited a smeared concentration of electrons (Figure 5), indicating minimal conjugation of the oxygen atoms with the aromatic rings (with the exception of O(4)). For every hydrogen bond, these lone pairs almost perfectly align with the O···H−O and O···H−C bond paths. Such lone pair regions and lack of conjugation of the OH group with the aromatic ring were previously observed in the electron density of estrone and estradiol.[12,13]

An additional feature of genistein in the solid state is the observation of two intermolecular H···H interactions between H(3′) and H(3′)^{v} and between H(6) and H(5′)^{ii}. A molecular graph representation of the H(3′) and H(3′)^{v} interaction is shown in Figure 6. A (3,−1) bond CP, a bond path, and corresponding virial path in the negative potential energy density[51] were all found. Such interactions have been found in other charge density studies[12,59,60] where it was shown that this interaction type may

(57) Espinosa, E.; Molins, E. *J. Chem. Phys.* **2000**, *113*, 5686.
(58) Gatti, G. *Z. Kristallogr.* **2005**, *220*, 399.
(59) Matta, C. F.; Hernández-Trujillo, J.; Tang, T.-H.; Bader, R. F. W. *Chem.—Eur. J.* **2003**, *9*, 1940 and references therein.

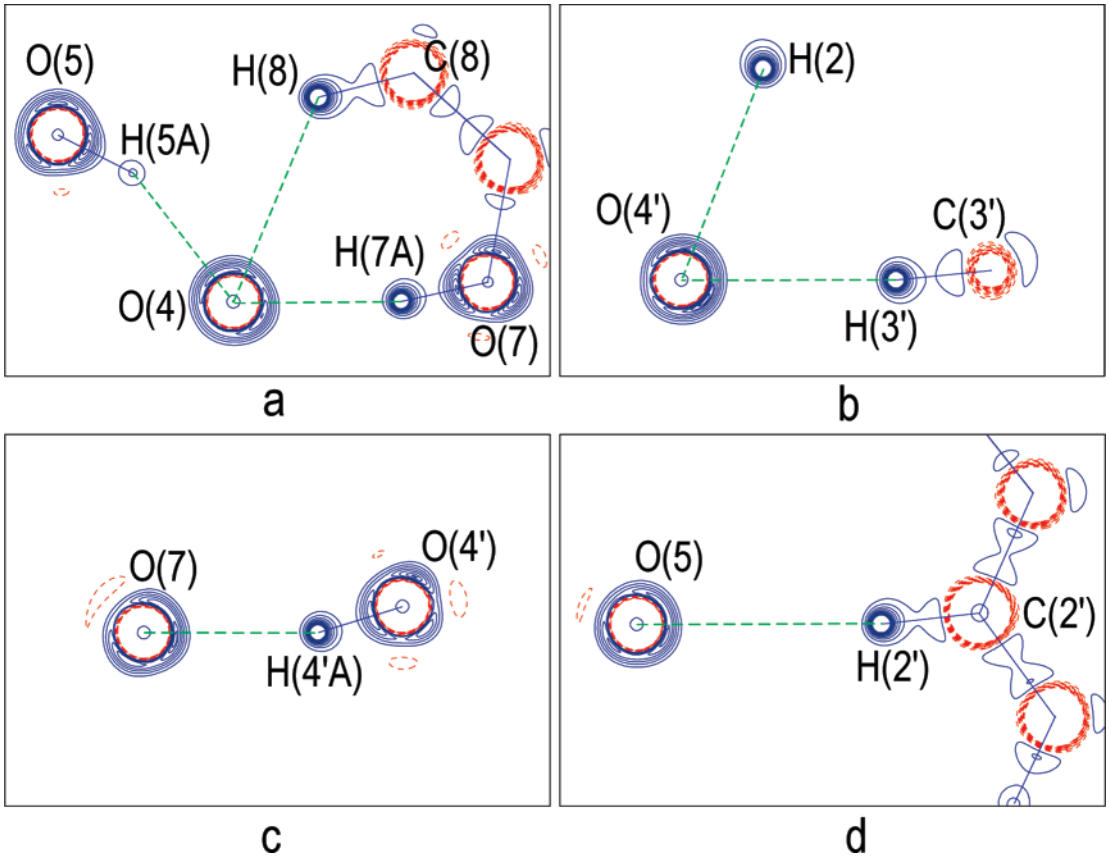

Figure 5. Laplacian maps showing the (a) O(4)···H(5A)−O(5), O(4)···H(7A)^{i}−O(7)^{i}, and O(4)···H(8)^{i}−C(8)^{i} hydrogen bonds; (b) O(4′)···H(3′)^{v}−C(3′)^{v} and O(4′)···H(2)^{iv}−C(2)^{iv} hydrogen bonds; (c) O(7)···H(4′A)^{ii}−O(4′)^{ii} hydrogen bond; and (d) O(5)···H(2′)^{iii}−C(2′)^{iii} hydrogen bond. Contour intervals are 17 e Å^{-5} with solid blue lines as negative and dashed red lines as positive. For symmetry operations see ref 53.

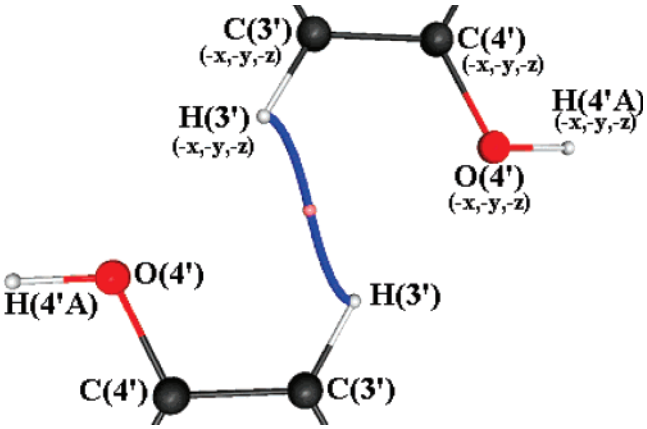

Figure 6. Molecular graph showing the H(3′)···H(3′)^{v} interaction between two different genistein molecules in the crystalline state. The H···H bond path is shown as a blue line while the (3,−1) bond critical point is shown as a pink circle.

make a stabilizing contribution of up to 10 kcal/mol to the molecular energy.[59] A positive Laplacian and positive total electronic energy density found at the bonding critical points indicate these to be closed-shell type interactions.

4.4. Atomic Charges. The atomic charge can be defined as the difference between the nuclear and electronic charges integrated over the atomic basins defined by zero flux surfaces:[38]

$$q(\Omega) = Z_{\Omega} - N(\Omega)$$

The experimental atomic charges sum to essentially zero indicating an electroneutral molecule, as required. Also, the volumes of the atomic basins were determined. On summation, there is only a 0.2% difference between the total volume and the value based on the volume of the unit cell divided by 8, the number of molecules in the unit cell (Table 3).

Chemically, most of the atomic charges determined from the AIM theory[38] are very reasonable (Table 3). All of the carbons bound to oxygens are highly positive as expected due to the polarization of the electrons toward the more electronegative oxygen. The quantitative differences between the carbons depend upon the type of bond they participate in with their respective oxygen. For example, the carbons (C(2) and C(8A)) bound to the C−O−C oxygen in the C ring are the least positive since they only form a single bond to oxygen. Conversely, the carbon (C(4)) bound to the carbonyl oxygen contains the largest positive charge due to the double bond character. All the other carbons and C−H hydrogens are either slightly positive or negative indicating that these atoms have charges close to zero. As expected, the O−H hydrogens are more positively charged (avg. 0.60 e^{-}) than the C−H hydrogens (avg 0.05 e^{-}). Furthermore, the atomic charges determined from the AIM theory[38] in this study were found to be similar to those for molecules studied in other recent charge density studies.[12,13,42,52]

An alternative measure of the atomic charges may be obtained from the monopole populations (P_v) which were refined as a

(60) Matta, C. F.; Castillo, N.; Boyd, R. J. *J. Phys. Chem.* **2006**, *B110*, 563.

Table 3. Atomic Charges and Volumes in the Genistein Crystal[a]

atom	$q(\Omega)_{AIM}$ (e$^-$)	$V(\Omega)_{AIM}$ (Å^3)	$q(P_v)$ (e$^-$)	q(Mulliken charge) (e$^-$)
O(7)	−1.05	17.29	−0.26	−0.35
O(5)	−1.00	19.48	−0.19	−0.34
O(1)	−0.99	15.91	−0.09	−0.28
O(4)	−1.03	16.66	−0.23	−0.42
O(4′)	−0.97	17.03	−0.21	−0.37
C(7)	0.44	8.34	0.08	0.18
C(6)	0.05	10.42	−0.07	−0.08
C(5)	0.56	7.61	0.12	0.22
C(4A)	−0.12	9.26	−0.05	−0.26
C(4)	0.92	6.49	0.01	0.39
C(3)	−0.01	10.05	0.02	−0.24
C(2)	0.39	10.65	−0.06	0.17
C(8A)	0.43	7.71	0.07	0.20
C(8)	0.00	11.26	−0.05	−0.12
C(1′)	−0.05	10.08	−0.05	−0.06
C(2′)	0.01	11.93	−0.02	−0.01
C(3′)	−0.09	13.20	−0.16	−0.10
C(4′)	0.41	8.84	0.06	0.16
C(5′)	−0.03	11.94	−0.09	−0.13
C(6′)	−0.03	12.66	−0.05	−0.06
H(6)	−0.02	7.05	0.03	0.12
H(2)	0.13	5.91	0.13	0.13
H(8)	0.10	6.47	0.08	0.10
H(2′)	0.05	7.81	0.05	0.10
H(3′)	0.14	6.27	0.16	0.11
H(5′)	−0.01	7.28	0.03	0.09
H(6′)	−0.02	7.64	0.00	0.09
H(7A)	0.62	1.60	0.27	0.26
H(5A)	0.59	1.82	0.24	0.25
H(4′A)	0.60	1.91	0.25	0.25
Σ	0.00	290.54[c]	0.00	0
L_{err}, au[b]	0.0005			
L_{max}, au	0.0009			

[a] $q(\Omega)$ and $V(\Omega)$ are atomic charges and volumes integrated over atomic basins, and $q(P_v)$ is a charge calculated from monopole populations. [b] $L_{err} = (\Sigma L_\Omega^2/N_{atoms})^{1/2}$, where L_Ω is the atomic integrated Lagrangian.[62] [c] Unit cell volume/8 = 291.18.

spherical part of the Hansen−Coppens multipole model. In general these charges reflect the same tendency as the integrated charge $q(\Omega)$, though being much lower in value as has been previously discussed.[52]

Theoretical Mulliken charges were also calculated using Gaussian98[61] on a single genistein molecule at the experimental geometry (DFT/B3LYP/6-311G(d,p)). As expected, the trends in the Mulliken charges are similar to those obtained from the experimental determinations with magnitudes closer to those obtained from the monopole populations.

Earlier studies of the estrogen receptor and its ligands have pointed to hydrogen bonds as the main type of bonding which would mediate the binding of genistein to the receptor.[36,63,64] The atomic charge of each atom indicates where strong hydrogen bonds can form to the ligand binding cavity of the estrogen receptor. For example, highly negative oxygens should act as acceptors when they form strong hydrogen bonds with positive O−H or N−H donor hydrogens of an amino acid residue, while the strongly positive hydroxyl hydrogens would form strong hydrogen bonds with a negative oxygen or nitrogen of an amino acid residue. The results from the crystal structure study of the

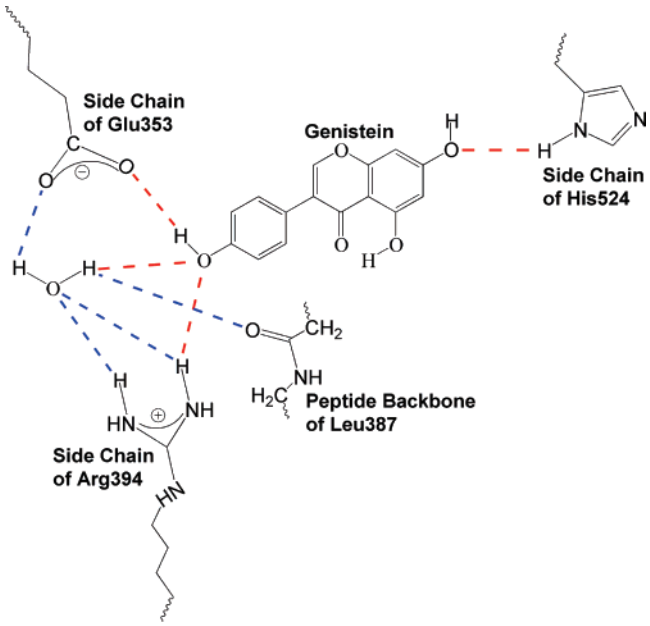

Figure 7. Representation of the hydrogen-bonding scheme of the ligand binding cavity of ER_α and genistein:[36,63,64] red lines involve genistein, and blue lines involve a water molecule considered to be an important part of the receptor structure.

estrogen receptor complexed with genistein confirm this argument (Figure 7).[63,64] It was shown that the negative O(4′), which has a charge of −0.97 e$^-$ in this study, forms strong hydrogen bonds with the positive O−H and N−H hydrogens of a solvent water molecule and an arginine residue in the ligand binding domain of the estrogen receptor, respectively. Also, the very positive hydroxyl H(4′A) hydrogen, which has a charge of 0.60 e$^-$, forms strong hydrogen bonds with the carbonyl oxygens of a glutamate residue. Finally, due to its negative charge (1.05 e$^-$), the O(7) oxygen acts as an acceptor in a hydrogen bond with the N−H hydrogen of a histidine residue.

4.5. Electrostatic Potential. Given the nuclear positions and the electron density distribution, the electrostatic potential (ESP) can be determined as follows:

$$V(\vec{r}) = \sum_A \frac{Z_A}{|\vec{R}_A - \vec{r}|} - \int \frac{\rho(\vec{r}')\, d\vec{r}'}{|\vec{r}' - \vec{r}|}$$

where Z_A is the charge on nucleus A located at the position R_A.[65] The ESP, particularly on the molecular surface, gives indications of how the molecule will approach and bind to other molecules or biological receptors. This approach includes hydrogen bonds and van der Waals interactions. As the intermolecular interactions in the crystal are complementary (i.e., a molecule in a crystal may be considered to be sitting in a cavity of complementary ESP), then this cavity must have ESP properties similar to those of a receptor if the molecule is strongly bound.

The ESP maps of genistein that were determined from experiment (molecule taken from the crystal) and theory (single molecule calculation) are shown as isosurfaces in Figure 8a and b, respectively. Although a theoretical calculation of the ESP of genistein has previously been reported[66] at the gas-phase

(61) Frisch, M. J. et al. *Gaussian 98*; Gaussian, Inc.: Pittsburgh, PA, 2004.
(62) Flensburg, C.; Madsen, D. *Acta Crystallogr.* **2000**, *A56*, 24.
(63) Manas, E. S.; Xu, Z. B.; Unwalla, R. J.; Somers, W. S. *Structure* **2004**, *12*, 2197.
(64) Pike, A. C. W.; Brzozowski, A. M.; Hubbard, R. E.; Bonn, T.; Thorsell, A.-G.; Engström, O.; Ljunggren, J.; Gustafsson, J.-Å.; Carlquist, M. *EMBO J.* **1999**, *18*, 4608.
(65) Coppens, P. *X-ray Charge Densities and Chemical Bonding*; Oxford University Press, 1997.
(66) Erkoç, F.; Erkoç, S. *THEOCHEM* **2002**, *583*, 163.

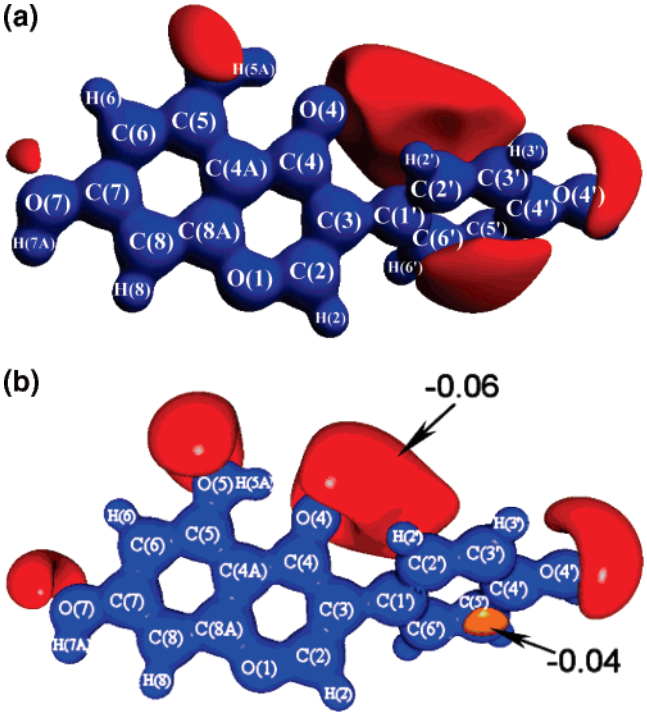

Figure 8. (a) Electrostatic potential isosurface of the genistein molecule in the crystalline state. The blue surface represents +1.0 e Å^{-1} while the red surface represents −0.10 e Å^{-1}. (b) Electrostatic potential isosurface of a single genistein molecule from the single molecule theoretical calculation at the experimental geometry. The blue surface represents +0.5 e Å^{-1}. Negative isosurfaces are in e Å^{-1} units as shown.

optimized geometry and using a minimal basis set, the report was lacking in detail. It was thus decided that a new calculation using a more extensive basis set and at the experimental geometry would be preferable to compare with the present experiment. We note that the ESPs are qualitatively similar in the experimental and theoretical cases. In both cases negative regions are located around the hydroxyl oxygens, the carbonyl oxygen, above and below the B aromatic ring, and to a lesser extent above and below the A and C rings. In agreement with some recently completed studies,[12,13,41,42,48,49] the ESP at similar chemical sites is quite transferable.

It has previously been shown[36,63,64] that the hydroxyl group at the C(4′) position of the B-ring of genistein mimics the phenolic group of the A-ring of estrone and estradiol-17β and the O(7)−H(7A) phenolic group of genistein on the A-ring mimics the hydroxyl group of the D-ring of estradiol-17β. Estrone,[12] estradiol-17β,[13] and genistein show negative ESP regions around the oxygens and above or below the aromatic rings. However, the ESP above and below the genistein A ring is significantly less negative than the B ring and, in fact, is quite comparable to that of the D ring in estradiol-17β.[13] Negative ESP regions were not observed around O(1) in agreement with a recent charge density of the furan ring in strychnine.[41] The negative regions can also be seen from the ESP mapped onto the molecular surface (Figure 9a and b).

As previously proposed, the experimental ESP can indicate how the ligand approaches a receptor.[69] Figure 7 represents the

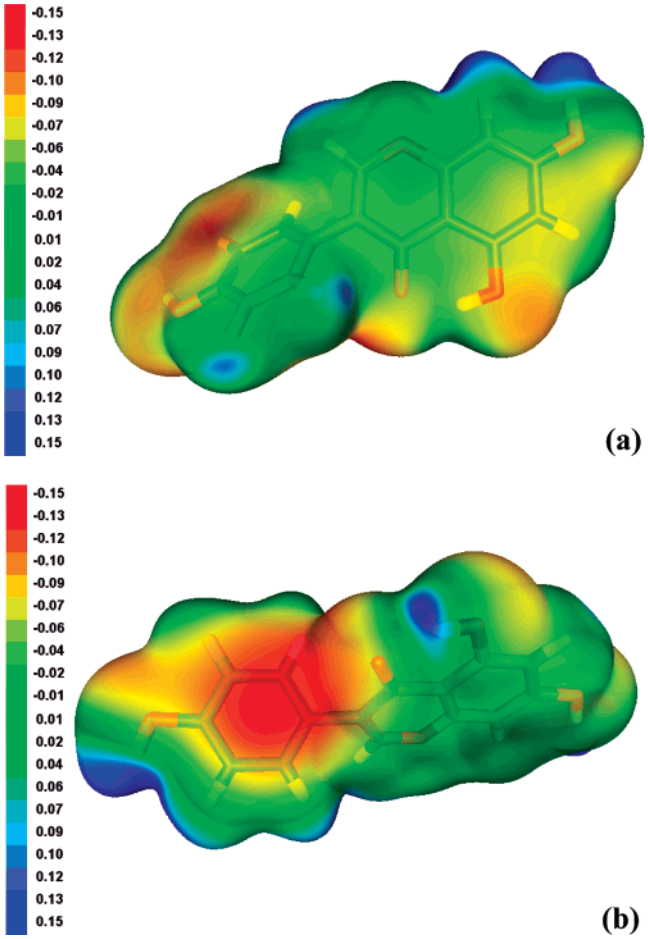

Figure 9. A view of the experimental electrostatic potential mapped on the molecular surface[67,68] ($\rho(r)$ = 0.001 au or 0.006 75 e Å^{-3}) (a) perpendicular to the planes of the A and C rings and (b) perpendicular to the plane of the B-ring. Units are e Å^{-1}.

ligand binding domain of ER$_\alpha$ and shows how genistein is proposed to form hydrogen bonds with the estrogen receptor.[36,63,64] It is argued that the negative ESP regions of genistein such as the region around the O(4′) oxygen should be initially attracted to the more positive Arg394 residue in the ligand binding cavity. Conversely, the positive ESP regions of genistein such as the regions surrounding the hydrogens, especially the hydroxyl hydrogen H(4′A), should be initially attracted to the more negative Glu353 residue in the ligand binding cavity. Furthermore, it is argued that these attractions driven by the ESP may provide the forces necessary to drive genistein toward the estrogen receptor in order to form the hydrogen bonds necessary for genistein to strongly bind to the receptor.

After the genistein approaches the estrogen receptor, the O(4′) oxygen should participate in a hydrogen bond with the positive hydrogens of the solvent water molecule and Arg394. Conversely, H(4′A) should participate in a hydrogen bond with the oxygens of the Glu353 residue of the receptor. Finally, at the front end of the ligand binding cavity, the negative electrostatic region of O(7) should initially be attracted to the positive His524 residue and thus form a hydrogen bond with the positive hydrogen of the histidine residue.

5. Conclusions

The electron density distribution, the topological properties of the electron density, and the electrostatic potential of genistein

(67) Laaksonen, L. *J. Mol. Graph.* **1992**, *10*, 33.
(68) Bergman, D. L.; Laaksonen, L.; Laaksonen, A. *Mol. Graph. Model.* **1997**, *15*, 301.
(69) Politzer, P.; Murray, J. S. *Theor. Chem. Acc.* **2002**, *108*, 134.

in the crystalline state have been determined. The results from this analysis agree well with studies on other agonistic steroids such as estrone[12] and estradiol-17β.[13]

Three relatively strong O···H−O hydrogen bonds, four weak O···H−C hydrogen bonds, and two intermolecular H···H interactions were characterized in this study. Based on the topological analysis, two of the O···H−O hydrogen bonds are considered to be incipient (partially covalent) bonding interactions and all of the rest of the O···H−O and O···H−C hydrogen bonds are pure closed-shell bonding interactions. A bond path and corresponding virial path were also found for the two H···H interactions.

Mapping of the electrostatic potential revealed negative regions around all the hydroxyl and carbonyl oxygens as expected from previous studies.[12,13,41,42,48,49] The negative regions are more pronounced and localized around the carbonyl oxygen in comparison to the hydroxyl oxygens. Also, extensive negative areas above and below the aromatic rings are observed which are the result of the π-electrons of the aromatic ring.

The ESP determined for genistein is in agreement with the proposed hydrogen-bonding scheme based on the crystal structure of the genistein/ER_α complex and is remarkably similar to that of estradiol-17β, despite the significant difference in molecular structure.

Acknowledgment. We thank Dr. A. Stash and Prof. V. Tsirelson for providing the *WinXPRO* program and the College of Arts and Sciences for support of the X-ray facility. We also thank Dr. A. Stash and Dr. B. L. Hanson for valuable discussions.

Supporting Information Available: Crystallographic and multipole refinement details, residual density plots, a plot of $\Sigma F_{obs}/\Sigma F_{calc}$ vs resolution, a normal probability plot, a complete list of closed-shell interactions, and complete citation for ref 61. This material is available free of charge via the Internet at http://pubs.acs.org.

JA075211J